Intelligent MPC for DFIG wind turbines

Amira Lakhdara[1], Tahar Bahi[2], Amina Azizi[1], Amina Benabda[1]
[1]Department of Electrotechnics, Badji Mokhtar-Annaba University, Annaba, Algeria
[2]LASA Laboratory, Department of Electrotechnics, Badji Mokhtar-Annaba University, Annaba, Algeria

Article Info

Article history:

Received Dec 16, 2025
Revised May 11, 2026
Accepted Jul 8, 2026

Keywords:

DFIG
Field-oriented control
Fuzzy-weighted MPC
Model predictive control
Wind turbine

ABSTRACT

This paper presents and evaluates advanced control strategies to enhance power tracking and robustness in doubly fed induction generator systems operating under realistic and perturbed wind conditions. In addition to the conventional field-oriented control, we develop a model predictive control approach that determines the optimal rotor voltage vectors by minimizing a quadratic cost function, as well as a fuzzy-weighted model predictive control in which the cost weight is adjusted online based on the tracking error and its derivative. The dynamic models used accurately represent the key behaviors of the doubly fed induction generator and its rotor-side and grid-side converters. MATLAB/Simulink simulations are carried out using two wind scenarios: a smooth sinusoidal profile and a filtered stochastic profile, while a robustness test introduces variations in rotor parameters during operation. The results demonstrate that the fuzzy-weighted model predictive control achieves faster convergence, lower steady-state error, and improved robustness, all while maintaining reasonable converter effort and acceptable power quality.

Corresponding Author:

Amira Lakhdara
Department of Electrotechnics, Badji Mokhtar-Annaba University
P.O.Box 12, Annaba 23000, Algeria
Email: amira.lakhdara@univ-annaba.dz

1. INTRODUCTION

The global energy transition relies heavily on renewable resources, with wind energy playing a key role. To meet grid requirements such as power quality, frequency stability, and grid-code compliance, wind turbines must operate reliably under variable wind conditions [1]. Doubly fed induction generators (DFIGs) remain widely used in onshore wind farms, accounting for over 58% of installations. Their advantage lies in partially rated converters and their ability to operate within ±30% of synchronous speed, enabling independent control of active and reactive power via rotor currents [2].

Since 2022, research has focused on improving the dynamic performance and robustness of DFIG systems under wind-speed disturbances. In 2024, a cascaded fuzzy power control (CFPC) strategy was proposed for multi-rotor wind turbines [3], using fuzzy inference on the rotor-side converter to enhance current quality and reduce THD without requiring an accurate model [4], [5], with reported reductions up to 47% and significant mitigation of active/reactive power ripples compared to PI-based control [5]-[8]. In 2025, a fractional fuzzy direct voltage control was introduced for standalone DFIGs [9], improving adaptability and stability under variable wind and load conditions [10], while another study showed that fuzzy control outperforms optimized PI in grid-connected DFIGs with faster response, lower overshoot, and reduced THD [11]. Overall, these works highlight the potential of intelligent control techniques to enhance robustness and power quality, although they often rely on complex tuning or fixed-weight strategies that limit adaptability. To address these limitations, this work introduces a predictive control strategy with adaptive fuzzy weighting applied to the rotor-side converter. Inspired by fuzzy regulation principles, the proposed method adjusts the cost-function weight in real time based on the tracking error and its derivative, behaving more aggressively during large deviations and more softly near steady state. The proposed controller is benchmarked against conventional field-oriented control (FOC) with PI regulators [12], [13] and classical MPC. The evaluation considers multiple wind profiles, smooth sinusoidal and filtered stochastic, and includes a robustness test under rotor-parameter variations.

The paper is organized as follows: i) Section 2 presents the DFIG and converter models and reviews PI-based FOC; ii) Section 3 introduces the control strategies (FOC/PI, classical MPC, and FW-MPC); iii) Section 4 discusses simulation results under random wind and parameter variations using RMSE, overshoot, and THD; and iv) Section 5 concludes the paper and outlines future work.

2. MODELING OF CONVERSION CHAIN

Figure 1 shows the block diagram of the wind energy conversion chain considered in this study. It depicts the conventional DFIG-based wind-turbine architecture and highlights the control layers evaluated (FOC, MPC, and FW-MPC). The main elements are:

- Mechanical stage: The WT supplies mechanical power to the DFIG via a gearbox, while an anemometer feeds the MPPT algorithm to generate the power reference.
- DFIG generator: The DFIG stator is directly connected to the grid, while the rotor is supplied through a back-to-back converter, enabling speed control and efficient energy capture with reduced losses [14].
- Rotor side converter (RSC): This voltage source inverter controls the rotor currents, regulating torque, speed, and reactive power in a d/q frame. FOC, MPC, and FW-MPC strategies are implemented on this converter [15].
- Grid side converter (GSC): The GSC shares the DC link with the RSC, transfers rotor power to the grid, regulates the DC-bus voltage and reactive power, and uses an R–L filter to reduce harmonics before the transformer [16].
- Grid interface: Stator and rotor powers are combined and injected into the grid through a transformer, ensuring near-unity power factor and good power quality. Overall, the system converts wind energy into electricity, with the RSC controlling speed/torque, the GSC regulating the DC link, and MPPT setting the power reference, enabling comparison of control strategies.

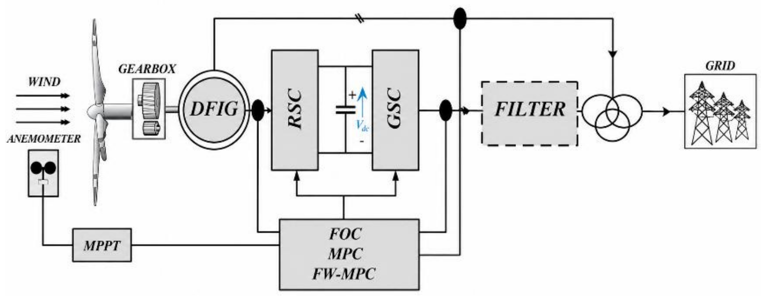

Figure 1. Conversion chain

2.1. Wind turbine modeling

Wind turbines convert wind energy into mechanical power. The mechanical power and the stator electric power output are computed as (1) and (2), respectively [17].

$$P_r = T_m.\omega_r \quad (1)$$

$$P_s = T_{em}.\omega_s \quad (2)$$

For a lossless generator, the mechanical equation is given by (3).

$$J\frac{d\omega_r}{dt} = T_m - T_{em} \quad (3)$$

In steady-state at fixed speed for a lossless generator:

$$T_m = T_{em} \quad (4)$$

and,

$$P_m = P_s + P_r \tag{5}$$

and therefore:

$$P_r = P_m - P_s = T_m.\omega_r - T_{em}.\omega_s = -sP_s \tag{6}$$

where s is the generator slip, defined by (7).

$$s = \frac{\omega_s - \omega_r}{\omega_s} \tag{7}$$

The remaining symbols are defined as follows: T_m: mechanical torque (N·m), ω_r: rotor angular speed (rad/s), ω_s: synchronous angular speed (rad/s), P_m: mechanical power (W), P_s: stator electrical power (W), and T_e: electromagnetic torque (N·m).

The theoretical value is well-known as the 'Betz limit' which determines the maximum power coefficient that can be extracted from a given wind speed and is defined by (8) [18].

$$C_p(\lambda, \beta) = 0.5176\left((\frac{116}{\lambda_I} - 0.4\beta - 5)e^{\frac{-21}{\lambda_i}} + 0.0068\lambda\right) \tag{8}$$

With (9):

$$\lambda = \frac{\omega_m.R}{V_w} \tag{9}$$

and (10).

$$\frac{1}{\lambda_i} = \frac{1}{\lambda + 0.08\beta} - \frac{0.035}{\beta^3 + 1} \tag{10}$$

The mechanical power will be written as (11) and (12).

$$P_m = C_p.P_e = \frac{1}{2}\rho\pi R^2 V_w^3 C_p(\lambda) \tag{11}$$

$$P_m = \frac{1}{2}\rho A V_w^3 C_p(\lambda, \beta) \tag{12}$$

where ρ: air density (kg/m^3), A: blades swept area, V_w: wind speed (m/sec), and C_P (λ,β): power coefficient, which is defined as the ratio of turbine power to wind power and is a function of the pitch angle (β) and tip speed ratio (λ). Taking into account the gearbox ratio K, then P_m of the electric generator equals:

$$P_m = \frac{1}{2}C_p\left(\frac{\omega_m R}{KV_m}\right)\rho\pi R^2 V_m^3 \tag{13}$$

2.2. Doubly fed induction machine modeling

The DFIG is equipped with a three-phase stator similar to that of a conventional induction machine. Its rotor also carries a three-phase winding, accessible through three slip rings and brushes [19], [20]. As shown in Figure 1, the stator is connected directly to the grid, whereas the rotor is interfaced to the same grid via power-electronic converters. The equivalent circuit of the DFIG is illustrated in Figure 2.

The mathematical modeling: the transformation matrix *P(θ)* is introduced to perform the *d-q* reference frame conversion [21]:

$$P(\theta) = \frac{2}{3}\begin{bmatrix} cos(\theta) & cos\left(\theta - \frac{2\pi}{3}\right) & cos\left(\theta + \frac{2\pi}{3}\right) \\ -sin(\theta) & -sin\left(\theta - \frac{2\pi}{3}\right) & -sin\left(\theta + \frac{2\pi}{3}\right) \end{bmatrix} \tag{14}$$

- Voltage equation

$$\begin{cases} V_{s,q} = R_s i_{s,q} + \frac{d\phi_{s,q}}{dt} + (\omega_e \phi_{s,d}) \\ V_{s,d} = R_s i_{s,d} + \frac{d\phi_{s,d}}{dt} - (\omega_e \phi_{s,q}) \end{cases} \tag{15}$$

$$\begin{cases} V_{r,q} = R_r i_{r,q} + \frac{d\phi_{r,q}}{dt} + (\omega_e - \omega_r)\phi_{r,d} \\ V_{r,d} = R_r i_{r,d} + \frac{d\phi_{r,d}}{dt} - (\omega_e - \omega_r)\phi_{r,q} \end{cases} \quad (16)$$

- Power equations

$$\begin{cases} P_s = \frac{3}{2}(V_{s,d} i_{s,d} + V_{s,q} i_{s,q}) \\ Q_s = \frac{3}{2}(V_{s,q} i_{s,d} - V_{s,d} i_{s,d}) \end{cases} \quad (17)$$

- Torque equation

$$T_e = \frac{-3p}{4}(\phi_{s,d} i_{s,q} - \phi_{s,q} i_{s,d}) \quad (18)$$

- Flux equations

$$\begin{cases} \phi_{s,d} = (L_{ls} + L_m) i_{s,d} + L_m i_{r,d} \\ \phi_{s,q} = (L_{ls} + L_m) i_{s,q} + L_m i_{r,q} \end{cases} \quad (19)$$

$$\begin{cases} \phi_{r,d} = (L_{lr} + L_m) i_{r,d} + L_m i_{s,d} \\ \phi_{r,q} = (L_{lr} + L_m) i_{r,q} + L_m i_{s,q} \end{cases} \quad (20)$$

With R_s: stator winding resistance (Ω), R_r: rotor winding resistance (Ω), L_{ls}: stator leakage inductance (H), L_{lr}: rotor leakage inductance (H), L_m: magnetizing inductance (H), ω_e: grid electrical angular frequency (rad/s), ω_r: rotor electrical angular frequency (rad/s), $V_{s,d}$, $V_{s,q}$: stator voltages in the direct (d) and quadrature (q) axes (V), $V_{r,d}$, $V_{r,q}$: rotor voltages in the direct (d) and quadrature (q) axes (V), $i_{r,d}$, $i_{r,q}$: rotor currents in the d/q axes (A), $i_{s,d}$, $i_{s,q}$: stator currents in the d/q axes (A), $\varphi_{s,d}$, $\varphi_{s,q}$: stator flux linkages in the d/q axes (Wb), $\varphi_{r,d}$, $\varphi_{r,q}$: rotor flux linkages in the d/q axes (Wb), and p: number of pole pairs.

In this configuration, the rotor-side converter (RSC) and grid-side converter (GSC) are voltage source converters based on IGBTs. The rotor is connected through slip rings to the converter, while the stator is directly connected to the grid. The DFIG converts wind energy into electrical power supplied via both the stator and the rotor. The inverter switching signals are generated using PWM by comparing a sinusoidal reference with a high-frequency triangular carrier.

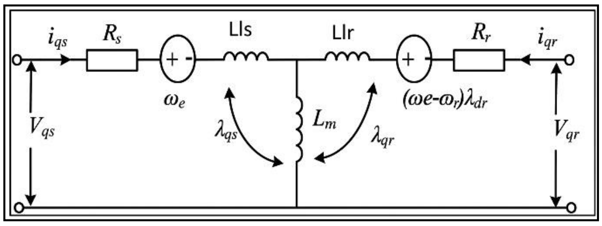

Figure 2. DFIG electrical model

2.3. Rotor side converter, grid side converter and DC bus

The modulation strategy (SVPWM/PWM) dictates $V_{r,dq}$ is bounded by $\|V_r\| \leq V_{max}$ [22], [23].

$$i_{RSC} = \frac{P_{RSC} \cdot 10^3}{V_{dc}} \quad (21)$$

$$i_{GSC} = -i_{RSC} \quad (22)$$

Where V_{max}: maximum voltage applied to the rotor and V_{dc}: DC bus voltage of the converter.

3. CONTROL SYSTEM

3.1. Field-oriented control

By decoupling active power (P) with $i_{r,q}$ and reactive power (Q) with $i_{r,d}$, the system enables the design of two independent PI controllers [24]-[26]:

$$\begin{cases} e_d = i_{r,d_{ref}} - i_{r,d} \\ e_q = i_{r,q_{ref}} - i_{r,q} \end{cases} \quad (23)$$

$$\begin{cases} i_{r,q_{ref}} = \frac{P_{ref}}{k_P} \\ i_{r,d_{ref}} = \frac{Q_{ref}}{k_Q} = 0 \end{cases} \quad (24)$$

$$\begin{cases} V_{r,d} = K_{p,d}.e_d + K_{i,d}\int e_d dt \\ V_{r,q} = K_{p,q}.e_q + K_{i,q}\int e_q dt \end{cases} \quad (25)$$

Where k_P, k_Q: gains linking the rotor current components to P and Q powers, P_{ref}, Q_{ref} : active and reactive power references, $i_{r,q,ref}$, $i_{r,d,ref}$: reference rotor currents, $K_{p,q}$, $K_{p,q}$, $K_{i,d}$, $K_{i,q}$: proportional and integral gains of the PI controllers in the field-oriented control, and e: tracking error.

3.2. Classical model predictive control

The discrete-time model with sampling period dt [27] is expressed as follows, starting from:

$$i = \frac{1}{L_r}(V - R_r i) \quad (26)$$

We have:

$$i(k+1) = i(k) + \alpha(V(k) - R_r i(k)) \quad (27)$$

With,

$$\alpha = dt/L_r \quad (28)$$

Quadratic criterion,

$$J = (i(k+1) - i_{ref}(k))^2 + \lambda(V(k) - V(k-1))^2 \quad (29)$$

$$V_{ref}(k) = \frac{\lambda V(k-1) - \alpha e(k) + \alpha^2 R_r i(k)}{\alpha^2 + \lambda} \quad (30)$$

Where J: cost function, λ: weighting factor that regulates the trade-off between tracking accuracy and control smoothness, α: ratio between the control sampling step and the rotor inductance, and k: sampling index.

3.3. Adaptive fuzzy-weighted predictive control

In the proposed FW-MPC, the weighting factor λ in the cost function is updated online based on the tracking error e (k) and its derivative de (k). Both variables are first normalized to the range [–1, 1] according to their maximum expected magnitudes. Five triangular membership functions are defined for each input (negative large, negative small, zero, positive small, and positive large).

The previous MPC law is retained, but the weighting factor *λ* is dynamically adapted according to the error and its derivative.

$$\lambda(e,\dot{e}) = \lambda_{\min} + (\lambda_{\max} - \lambda_{\min})\exp(-k_e|e| - k_d|\dot{e}|) \quad (31)$$

With, $0 < \lambda_{min} < \lambda_{max}$ and k_e, $k_d > 0$. The resulting control law is:

$$V_{ref}(k) = \frac{\lambda(e,\dot{e})V(k-1) - \alpha e(k) + \alpha^2 R_r i(k)}{\alpha^2 + \lambda(e,\dot{e})} \quad (32)$$

This law is applied separately to the d and q axes using λ_d and λ_q, respectively.

4. SIMULATION RESULTS

In this section, simulation results are presented for a random wind speed profile scenario, followed by an evaluation of the system performance using standard performance metrics [28-30]. The detailed specifications of the system components and control parameters used in the simulations are summarized in Tables 1–3. Specifically, Table 1 presents the main parameters of the electromechanical components, including the wind turbine, gearbox, and DFIG. Table 2 summarizes the specifications of the power converters, DC bus, filter, transformer, grid, and load. Finally, Table 3 lists the main control parameters used in the proposed control strategy, including the FOC-PI and FW-MPC parameters. These parameters are used throughout the simulations to evaluate the dynamic performance and robustness of the proposed control approach.

Table 1. Electromechanical components

Block	Parameter	Symbole	Value	Unit
Turbine	Air density	ρ	1.225	$Kg\cdot m^{-3}$
Turbine	Rotor radius	R	40	m
Turbine	Optimal power coefficient	$C_{p,opt}$	0.46	–
Turbine	Optimal tip speed ratio	λ_{opt}	8.0	–
Reducer	Ratio	G	90	–
DFIG	Rated power	P_{rated}	6	KW
DFIG	Pole pairs	p	2	–
DFIG	Stator resistance	R_s	0.40	Ω
DFIG	Rotor resistance	R_r	0.38	Ω
DFIG	Stator leakage inductance	$L_{\ell s}$	3.0e-3	H
DFIG	Rotor leakage inductance	$L_{\ell r}$	3.0e-3	H
DFIG	Magnetizing inductance	L_m	80e-3	H

Table 2. Converters, DC bus, filter, grid and load

Block	Parameter	Symbole	Value	Unit
DC bus	Voltage	V_{dc}	600	V
DC bus	Capacitance	C_{dc}	$4e\text{-}^{3}$	F
RSC	Switching frequency	$f_{sw,R}$	$5e^{3}$	Hz
RSC	Sampling period	$T_{s,R}$	$100e\text{-}^{6}$	s
GSC	Switching frequency	$f_{sw,G}$	$5e^{3}$	Hz
GSC	Sampling period	$T_{s,G}$	$100e\text{-}^{6}$	s
Filter	Series inductance	L_f	$2.0e^{-3}$	H
Filter	Series resistance	R_f	0.20	Ω
Transformer	LV side voltage (LL)	V_{LV}	0.4	KV
Transformer	Turns ratio (LV/HV)	n	0.4/11	–
Grid	Voltage (LL)	V_G	400	V
Grid	Frequency	f_0	50	Hz
DC bus	Voltage	V_{dc}	600	V
DC bus	Capacitance	C_{dc}	$4e^{-3}$	F

Table 3. Control parameters

Block	Parameter	Symbole	Value	Unit
FOC	PI gain $K_{p(i\_d)}$	$K_{p,id}$	5.0	–
FOC	PI gain $K_{i(i\_d)}$	$K_{i,id}$	50.0	s^{-1}
FOC	PI gain $K_{p(i\_q)}$	$K_{p,iq}$	5.0	–
FOC	PI gain $K_{i(i\_q)}$	$K_{i,iq}$	50.0	s^{-1}
MPC	Cost weighting factor	λ_{mpc}	$1e^{-3}$	–
FW-MPC	λ_{min}	λ_{min}	$5e^{-5}$	–
FW-MPC	λ_{max}	λ_{max}	$5e^{-3}$	–
FW-MPC	Adaptation gain	k_λ	3.0	–

4.1. Conversion chain parameters

The wind speed profile is shown in Figure 3. The wind oscillates around an almost constant mean value, with fast variations resembling filtered noise. This rich frequency content excites the DFIG dynamics and highlights the controllers' ability to attenuate high-frequency disturbances.

In Figure 4, all three controllers (FOC/PI, classical MPC, and fuzzy adaptive-weighted FW-MPC) successfully track the active power reference P_{ref} without drift. Regarding power error, dispersion is the largest with FOC/PI, intermediate with classical MPC, and smallest with FW-MPC (the error cloud being noticeably tighter). Reactive power remains close to zero ($Q \approx 0$) throughout the test, confirming effective active/reactive decoupling despite rapid fluctuations. The adaptive weighting function $w(e, \dot{e})$ in FW-MPC filters fast error components more effectively, while still maintaining accurate reference tracking.

Table 4 compares the power tracking performance of the three controllers under a random wind profile. The PI-based FOC shows the slowest response, the highest overshoot (4.0%), and the largest error values, confirming its limited robustness. The classical MPC improves both rise time and error indices, cutting the IAE by nearly one third compared to PI. The FW-MPC provides the best overall performance, with the fastest response (0.15 s), minimal overshoot (0.8%), and the lowest RMS (0.07) and IAE (0.68) values, demonstrating its superior capability to handle rapid fluctuations.

Figures 5 and 6 show that the rotor current i_{rq} follows the torque demand with small oscillations due to wind variations, while i_{rd} remains close to zero, confirming proper magnetization control. At the same time, v_{rq} reflects active power fluctuations without saturation. Although all controllers exhibit similar behavior, FW-MPC slightly reduces current peaks and variability, leading to lower stress, while also ensuring smoother voltage with reduced variance and no high-frequency artifacts, thus preserving converter margins.

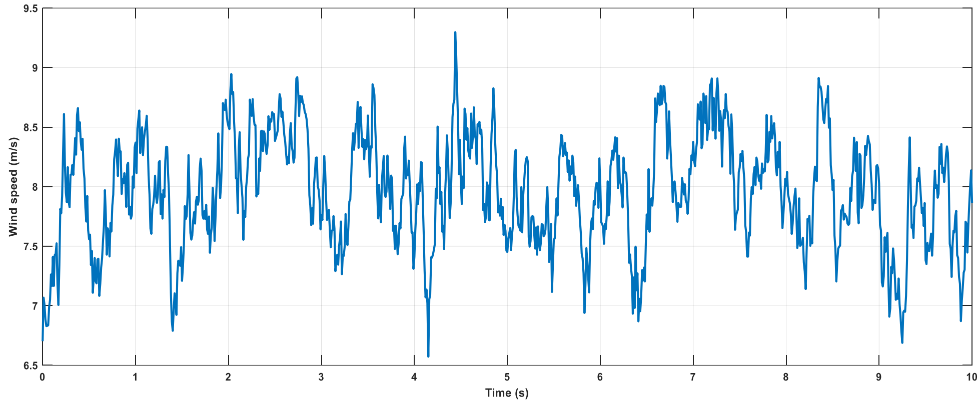

Figure 3. Random wind speed profile

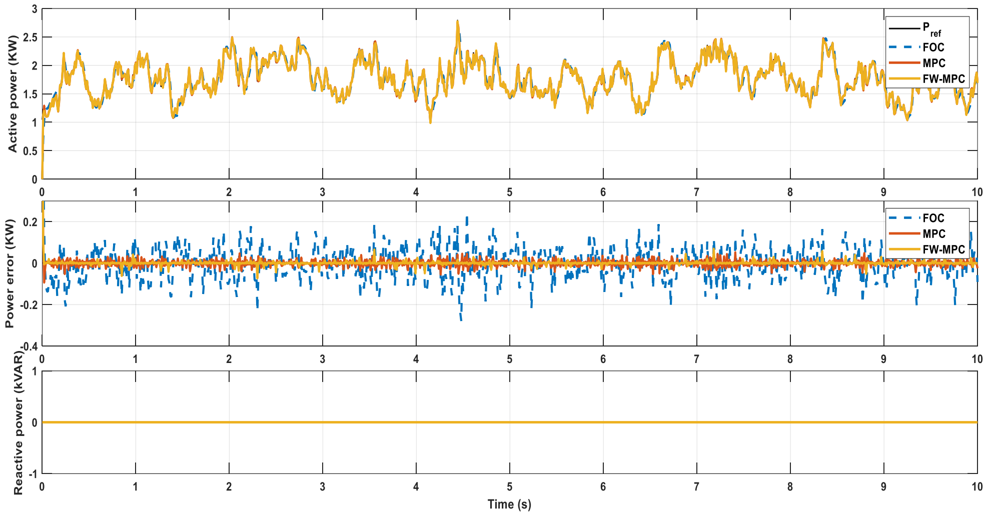

Figure 4. Active and reactive powers

Table 4. Power tracking performance (qualitative)

Controller	Rise time (s)	Overshoot (%)	RMS error at peaks (KW)	RMSE (KW)	IAE (KW·s)
FOC/PI	0.22	4.0	0.18	0.20	1.35
Classical MPC	0.18	2.2	0.11	0.13	0.92
FW-MPC	0.15	0.8	0.07	0.09	0.68

Table 5 compares control effort under disturbed wind conditions. The PI controller exhibits the highest effort with large voltage variance and current stress. Classical MPC reduces these peaks and slightly improves the power factor. FW-MPC achieves the smoothest control, with the lowest RMSE, reduced variance, minimal current peaks, and unity power factor, confirming its superior efficiency and robustness.

Figure 7 shows a parametric variation at ≈5 s (changes in R_r and L_r), where all controllers maintain active power tracking. However, the error response differs: FOC/PI exhibits the largest peaks and oscillations, classical MPC improves damping, while FW-MPC achieves the smallest error and fastest recovery. This is due to its adaptive weighting $w(e,\dot{e})$, which provides effective damping, aggressive during error growth and conservative during decay, thus reducing overshoot and ensuring smoother convergence.

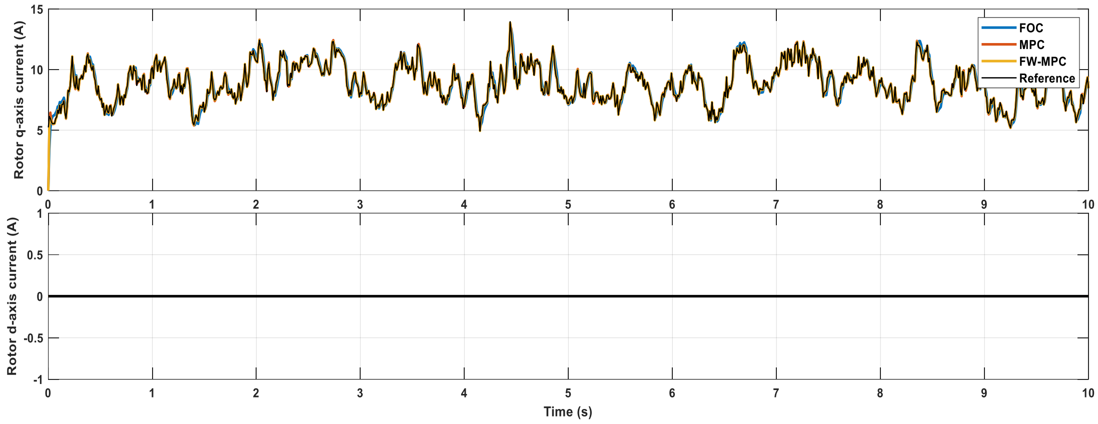

Figure 5. Rotor d- and q-axis currents

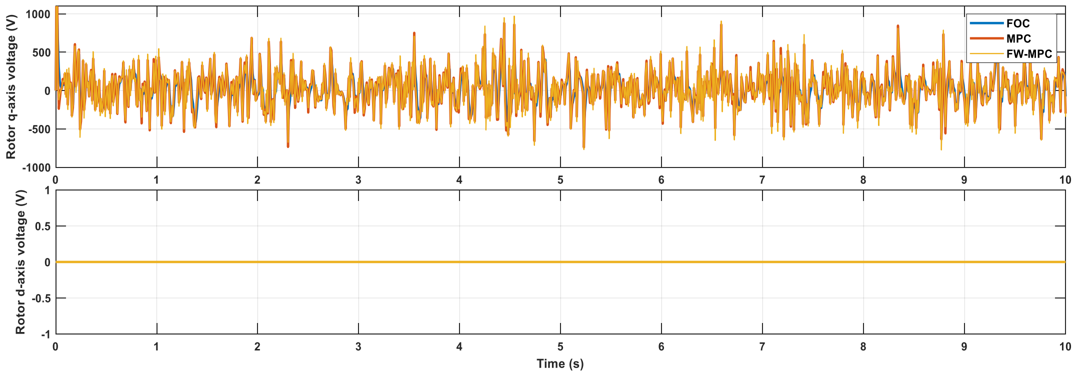

Figure 6. Rotor d- and q-axis voltages

Table 5. Control effort and constraints (qualitative)

Controller	$RMSE_{fast}$ (KW)	Var(v_{rq}) (V^2)	Peak v_{rq} (V)	Peaki_{rq} (A)	Mean$\lvert i_{rd}\rvert$ (A)	PFmean
FOC/PI	0.24	$1.10e^5$	900	12.2	0.035	0.998
Classical MPC	0.16	$0.95e^5$	850	11.9	0.030	0.999
FW-MPC	0.12	$0.85e^5$	820	11.7	0.025	0.999

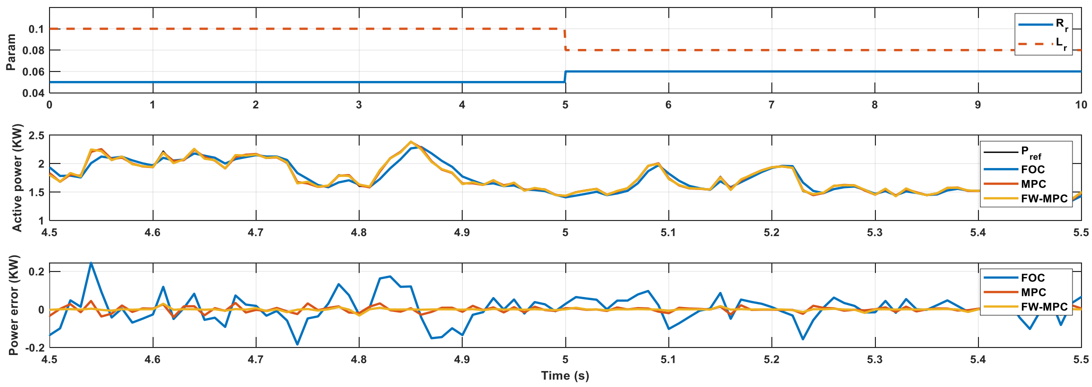

Figure 7. Active power with R_r increase and L_r decrease

Figure 8 presents the grid-side voltage and current. The grid voltage remains sinusoidal, stable (50 Hz), and unaffected by the choice of controller. The grid current follows the active power reference, maintaining phase alignment with no low-frequency distortions during the parameter jump. Zoomed views (three cycles) confirm nearly perfect superposition in both amplitude and phase across all three controllers.

Tables 6 and 7 show that all controllers maintain the same grid voltage (325 V), while FW-MPC delivers slightly higher current, indicating improved power transfer. It also achieves the best current quality, with the lowest THD (1.5%) and reduced noise, while preserving the 50 Hz fundamental. These results confirm the superior performance of FW-MPC for efficient and high-quality grid interaction.

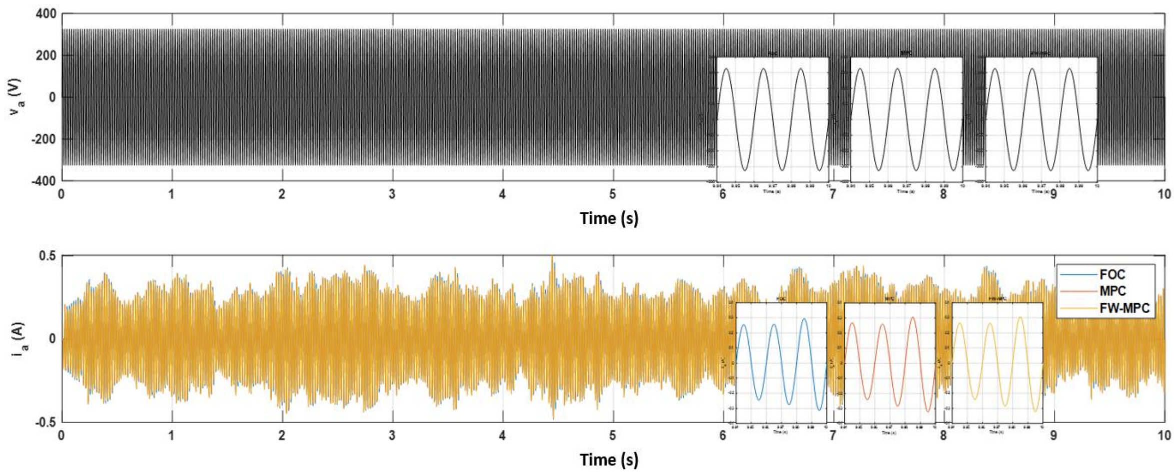

Figure 8. Grid-side voltage and current (GSC)

Table 6. Grid quantities

Controller	$V_{a,pk}$(V)	$I_{a,pk}$(A)	$I_{a,rms}$(A)
FOC/PI	325	0.28	0.198
Classical MPC	325	0.28	0.198
FW-MPC	325	0.30	0.212

Table 7. Current quality

Contrôleur	THD_i(%)	Background noise	$\sigma(i_a)$ over 1 s (A)
FOC/PI	2.2	0.0060	0.030
Classical MPC	1.8	0.0045	0.024
FW-MPC	1.5	0.0040	0.021

5. CONCLUSION

This study demonstrates the effectiveness of the proposed FW-MPC strategy. Under both sinusoidal and noisy wind conditions, it reduces RMSE, overshoot, and convergence time compared to FOC and classical MPC. It also ensures smoother rotor currents and voltages, lowering losses and thermal stress. The DFIG maintains near-unity power factor and acceptable THD. Robustness is confirmed under parameter variations and stochastic wind, with reduced peak errors and faster recovery. These results align with recent studies highlighting the benefits of adaptive MPC for improving performance and robustness in DFIG systems.

FUNDING INFORMATION

Authors state no funding involved.

AUTHOR CONTRIBUTIONS STATEMENT

This journal uses the Contributor Roles Taxonomy (CRediT) to recognize individual author contributions, reduce authorship disputes, and facilitate collaboration.

Name of Author	C	M	So	Va	Fo	I	R	D	O	E	Vi	Su	P	Fu
Amira Lakhdara	✓	✓	✓	✓	✓	✓		✓	✓	✓			✓	
Tahar Bahi		✓		✓		✓		✓	✓	✓	✓	✓		
Amina Azizi		✓	✓	✓			✓			✓	✓	✓		✓
Amina Benabda					✓		✓			✓		✓		✓

C : **C**onceptualization
M : **M**ethodology
So : **So**ftware
Va : **Va**lidation
Fo : **Fo**rmal analysis
I : **I**nvestigation
R : **R**esources
D : **D**ata Curation
O : Writing - **O**riginal Draft
E : Writing - Review & **E**diting
Vi : **Vi**sualization
Su : **Su**pervision
P : **P**roject administration
Fu : **Fu**nding acquisition

CONFLICT OF INTEREST STATEMENT

Authors state no conflict of interest.

DATA AVAILABILITY

The data that support the findings of this study are available from the corresponding author, upon reasonable request.

REFERENCES

[1] H. Badihi, Y. Zhang, B. Jiang, P. Pillay, and S. Rakheja, "A comprehensive review on signal-based and model-based condition monitoring of wind turbines: fault diagnosis and lifetime prognosis," *Proceedings of the IEEE*, vol. 110, no. 6, pp. 754–806, Jun. 2022, doi: 10.1109/JPROC.2022.3171691.

[2] H. Soleimani, D. Habibi, M. Ghahramani, and A. Aziz, "Strengthening power systems for net zero: a review of the role of synchronous condensers and emerging challenges," *Energies*, vol. 17, no. 13, 2024, doi: 10.3390/en17133291.

[3] H. Benbouhenni, N. Bizon, M. I. Mosaad, I. Colak, A. B. Djilali, and H. Gasmi, "Enhancement of the power quality of dfig-based dual-rotor wind turbine systems using fractional order fuzzy controller," *Expert Systems with Applications*, vol. 238, p. 121695, Mar. 2024, doi: 10.1016/j.eswa.2023.121695.

[4] K. F. Sayeh, S. Tamalouzt, D. Ziane, A. Bekhiti, and Y. Belkhier, "Utilizing fuzzy logic control and neural networks based on artificial intelligence techniques to improve power quality in doubly fed induction generator-based wind turbine system," *International Journal of Energy Research*, vol. 2025, no. 1, 2025, doi: 10.1155/er/5985904.

[5] K. F. Sayeh, S. Tamalouzt, D. Ziane, N. Benyahia, and S. L. Belaid, "A novel fuzzy-logic-improved direct power control strategy for DFIG-based wind turbine through real-time OPAL-RT validation," *International Journal of Electrical Power & Energy Systems*, vol. 172, p. 111317, Nov. 2025, doi: 10.1016/j.ijepes.2025.111317.

[6] H. Benbouhenni, I. Colak, N. Bizon, M. I. Mosaad, and T. G. Tella, "Power regulation of variable speed multi rotor wind systems using fuzzy cascaded control," *Scientific Reports*, vol. 14, no. 1, 2024, doi: 10.1038/s41598-024-67194-4.

[7] H. Benbouhenni, D. Zellouma, N. Bizon, and I. Colak, "A new PI(1 +PI) controller to mitigate power ripples of a variable-speed dual-rotor wind power system using direct power control," *Energy Reports*, vol. 10, pp. 3580–3598, Nov. 2023, doi: 10.1016/j.egyr.2023.10.007.

[8] M. Hichem and B. Tahar, "Fuzzy monitoring of stator and rotor winding faults for DFIG used in wind energy conversion system," *International Journal of Modelling, Identification and Control*, vol. 27, no. 1, pp. 49–57, 2017, doi: 10.1504/IJMIC.2017.082485.

[9] F. Boucetta *et al.*, "Robust direct voltage control of stand-alone DFIG wind systems using a fractional-order fuzzy logic approach," *Scientific Reports*, vol. 15, no. 1, p. 28762, Aug. 2025, doi: 10.1038/s41598-025-11910-1.

[10] K. Ullah *et al.*, "Wind farms and flexible loads contribution in automatic generation control: an extensive review and simulation," *Energies*, vol. 16, no. 14, 2023, doi: 10.3390/en16145498.

[11] M. Bahgat, M. Ezzat, M. A. Attia, S. F. Mekhamer, and N. M. Elbehairy, "Comparative analysis of pi and fuzzy logic controller for grid connected wind turbine under normal and fault conditions," *Scientific Reports*, vol. 15, no. 1, p. 1954, Jan. 2025, doi: 10.1038/s41598-024-85073-w.

[12] B. Wadawa, Y. Errami, A. Obbadi, S. Sahnoun, E. Chetouani, and M. Aoutoul, "Comparative application of the self-adaptive fuzzy-pi controller for a wind energy conversion system connected to the power grid and based on dfig," *International Journal of Dynamics and Control*, vol. 10, no. 6, pp. 2151–2173, Dec. 2022, doi: 10.1007/s40435-022-00952-2.

[13] A. Achar, Y. Djeriri, H. Benbouhenni, R. Bouddou, and Z. M. S. Elbarbary, "Modified vector-controlled dfig wind energy system using robust model predictive rotor current control," *Arabian Journal for Science and Engineering*, vol. 50, no. 14, pp. 11065–11089, Jul. 2025, doi: 10.1007/s13369-024-09310-0.

[14] A. A. Ansari and G. Dyanamina, "Fault ride-through operation analysis of doubly fed induction generator-based wind energy conversion systems: a comparative review," *Energies*, vol. 15, no. 21, 2022, doi: 10.3390/en15218026.

[15] S. R. Mosayyebi, S. H. Shahalami, and H. Mojallali, "Fault ride-through capability improvement in a dfig-based wind turbine using modified ADRC," *Protection and Control of Modern Power Systems*, vol. 7, no. 1, 2022, doi: 10.1186/s41601-022-00272-9.

[16] A. Memon, "Improved vector control methods for brushless double fed induction generator during inductive load and fault conditions," Universiti Teknologi Malaysia, 2022.

[17] L. Amira, B. Tahar, and M. Abdelkrim, "Strategy of sliding mode control wind energy conversion system," *International Journal of Engineering Science and Application*, vol. 4, no. 4, 2020.

[18] A. Tanvir, A. Merabet, and R. Beguenane, "Real-time control of active and reactive power for doubly fed induction generator (DFIG)-based wind energy conversion system," *Energies*, vol. 8, no. 9, pp. 10389–10408, Sep. 2015, doi: 10.3390/en80910389.

[19] P. Meena, V. Prema, M. S. Bhaskar, and D. Almakhles, "Bi-furcated stator winding configuration in three-phase induction generators for wind power generation," *IEEE Access*, vol. 9, pp. 153188–153198, 2021, doi: 10.1109/ACCESS.2021.3127526.

[20] A. Boukadoum, T. Bahi, and A. Bouguerne, "Power quality improvement using fuzzy logic controlled voltage source PWM rectifiers," *International Journal of Intelligent Engineering Informatics*, vol. 5, no. 3, p. 242, 2017, doi: 10.1504/ijiei.2017.086611.

[21] A. A. Chhipą *et al.*, "Modeling and control strategy of wind energy conversion system with grid-connected doubly-fed induction generator," *Energies*, vol. 15, no. 18, 2022, doi: 10.3390/en15186694.

[22] P. K. Nirala, R. Bhushan, and K. M. Jagtap, "Impact of grid-side converter filter on the small-signal stability of a grid-connected dfig-based wind-driven system," *International Journal of Circuit Theory and Applications*, vol. 53, no. 11, pp. 6621–6637, 2025, doi: 10.1002/cta.4464.

[23] S. Lu *et al.*, "Space vector pulse width modulation strategy for modular multilevel converters in power system," *IET Cyber-Physical Systems: Theory & Applications*, vol. 8, no. 3, pp. 186–194, Sep. 2023, doi: 10.1049/cps2.12052.

[24] H. Gasmi, H. Benbouhenni, I. Colak, T. Tafticht, and N. Bizon, "Using the proportional dual integral strategy to improve the characteristics of the indirect field-oriented control of DFIG-based wind turbine systems," *e-Prime - Advances in Electrical Engineering, Electronics and Energy*, vol. 9, p. 100749, Sep. 2024, doi: 10.1016/j.prime.2024.100749.

[25] A. Radaideh, M. Bodoor, and A. Al-Quraan, "Active and reactive power control for wind turbines based DFIG using LQR controller with optimal gain-scheduling," *Journal of Electrical and Computer Engineering*, vol. 2021, pp. 1–19, Oct. 2021, doi: 10.1155/2021/1218236.

[26] F.-E. Blouh, M. Bezza, and A. El Azzab, "Fuzzy logic–based control with MPPT for power quality enhancement in DFIG wind energy systems," *International Journal of Robotics and Control Systems*, vol. 5, no. 6, pp. 2750–2766, Nov. 2025, doi: 10.31763/ijrcs.v5i6.2185.

[27] H. Chojaa *et al.*, "Robust control of DFIG-based WECS integrating an energy storage system with intelligent MPPT under a real wind profile," *IEEE Access*, vol. 11, pp. 90065–90083, 2023, doi: 10.1109/ACCESS.2023.3306722.

[28] S. Yan, J. Chen, M. Wang, Y. Yang, and J. M. Rodriguez, "A survey on model predictive control of dfigs in wind energy conversion systems," *CSEE Journal of Power and Energy Systems*, vol. 10, no. 3, pp. 1085–1104, 2024, doi: 10.17775/CSEEJPES.2022.08500.

[29] A. Bahi, S. Bentrad, and I. Gasmi, "Study the impact of homomorphic encryption on the accuracy of recommendation systems in e-commerce," in *International Conference on Advanced Engineering in Petrochemical Industry (ICAEPI'23)*, 2023, pp. 28–30.

[30] Y. Liu, Y. Zhou, S. Wen, and C. Tang, "A strategy on selecting performance metrics for classifier evaluation," *International Journal of Mobile Computing and Multimedia Communications*, vol. 6, no. 4, pp. 20–35, 2014, doi: 10.4018/IJMCMC.2014100102.

BIOGRAPHIES OF AUTHORS

Amira Lakhdara an associate professor in electrical engineering at Badji Mokhtar Annaba University, Algeria. She received her engineering and master's degrees from the same university and her Ph.D. in renewable energy from 8 May 1945 Guelma University in 2022. Her research focuses on electrical drives, power electronics, and AI applications in renewable energy systems. She can be contacted at email: amira.lakhdara@univ-annaba.dz.

Tahar Bahi is a professor in electrical engineering at Badji Mokhtar Annaba University, Algeria. He received his engineering, magister, and doctorate degrees in electrical engineering from the same university in 1983, 1986, and 2006, respectively. His research focuses on electrical drives, power electronics, fault diagnosis, and AI applications in renewable energy systems. He can be contacted at email: tahar.bahi@univ-annaba.dz.

Amina Azizi is an associate professor in electrical engineering at Badji Mokhtar Annaba University, Algeria. She received her master's and Ph.D. degrees in electrical engineering from the same university in 2014 and 2019, respectively. Her research focuses on electrical drives, power electronics, and AI applications in renewable energy systems. She can be contacted at email: amina.azizi@univ-annaba.dz.

Amina Benabda is an associate professor in electrical engineering at Badji Mokhtar Annaba University, Algeria. She received her master's and Ph.D. degrees in electrical engineering from the same university in 2014 and 2018, respectively. Her research focuses on electrical drives, power electronics, and AI applications in renewable energy systems. She can be contacted at email: amina.benabda@univ-annaba.dz.